Ultraviolet-A light/oligomeric melem vs. visible light/graphitic carbon nitride towards H₂O₂ photo-production and pollutants degradation: sometimes less is more

Iván Sciscenko [a,*], Arianna Actis [b], Enrico Salvadori [b], Antonio Arques [a], Claudio Minero [b,c], Fabrizio Sordello [b], Marco Minella [b,c]

[a] Universitat Politècnica de València, Departamento de Ingeniería Textil y Papelera, Plaza Ferrándiz y Carbonell s/n, Alcoy 03801, Spain
[b] Università di Torino, Dipartimento di Chimica, Via Pietro Giuria 7, Torino 10125, Italy.
[c] NIS, Nanomaterials for Industry and Sustainability, Inter-departmental Centre, University of Turin, Via Quarello 15, Torino 10135, Italy

ARTICLE INFO

ABSTRACT

Currently, there is a convention on performing photocatalytic reactions with graphitic carbon nitride (g-C₃N₄) with visible light only, in spite of the synthesis efforts required to obtain acceptable results on its applications. Therefore, in this work, we have compared the photocatalytic performance, under UVA and visible light irradiation, of carbon nitrides prepared from melamine calcination at different temperatures, 350 – 650 °C, by means of H₂O₂ photo-production (with methanol as hole scavenger) and of photocatalytic phenol oxidation, respectively. The photocatalysts were characterised by several techniques, and Principal Component Analysis (PCA) was employed to highlight correlations among the huge amount of generated data and obtain rapid conclusions on the overall trend. Results demonstrated that the compound obtained from melamine calcination at 425 °C (oligomeric melem) under UVA irradiation led to an outstanding 2 mM h^{-1} H₂O₂ production rate in presence of 3 M of methanol, as well as the fastest phenol 100 µM oxidation rates ($k_{obs} = 4 \times 10^{-2}$ min^{-1}); higher polymerisation temperatures (i.e., lower band gap energies, C:N ≈ 3:4) resulted in lower photocatalytic behaviours under UVA irradiation. Furthermore, the PCA indicated that the presence of melem oligomers in any material was detrimental to observe high photocatalytic activities, being negligible in those with scarce polymerisation degree (melam oligomer) or high one (melon). Taking advantage of UV lamps and low molecular weight carbon nitride materials, we believe that a change in the literature focus should be done due to the here reported advantages of UVA/oligomeric melem system over the visible light/g-C₃N₄ one.

1. Introduction

Carbon nitride (known as C₃N₄) is a highly-stable metal-free semiconductor gaining momentum as the fourth generation of heterogeneous photocatalyst [1–3]. Its graphitic structure (g-C₃N₄) is among its most stable allotrope at ambient conditions, composed by layered polymeric heptazine networks arranged in honeycomb configurations. As well as with graphite, the layers interact by weak van der Waals forces, allowing easy exfoliation into individual 2D sheets [4].

This semiconductor is usually prepared by thermal polycondensation, placing a certain amount of a precursor (typically melamine, cyanamide, urea) in a covered crucible, followed by heating in air or anoxic atmosphere (e.g., N₂, NH₃, H₂) at controlled temperature (usually in the range of 500–650 °C) [5]. It is widely reported that the nature of the precursor, final temperature, and adopted ramp strongly affect the physico-chemical properties of the obtained material, eventually reflected on photocatalytic activity changes [6]. As a matter of fact, the C:N ratio of 3:4 is more a convention rather than a real stoichiometric identification, reflected on the presence of considerable amounts of hydrogen and reported ratios sensitive only to the applied

temperature, being more consistent with the composition of Liebig's melon ($C_6N_9H_3$) [7]. The presence of hydrogen indicates incomplete condensed structures from primary and/or secondary amine groups (-NH and -NH$_2$, respectively) on the terminating edges. This could not necessarily be a drawback, as these defects (in other words, the presence of lower condensed carbon-nitride structures, i.e. melam, melem) are believed to promote a Lewis-base character towards metal-free coordination chemistry, being the real active sites of these materials [8–10], as well increasing their hydrophilicity [11].

The energy bands location of g-C$_3$N$_4$ (or g-CN from now on, based on the aforementioned statements regarding the inaccurately established stoichiometry) also add ambiguity towards the final application. While this material has favourable conduction band (CB) edge positions ($\approx$ -1.2 V vs. NHE) for reductive reactions (e.g., H$_2$O$_2$ photo-production [12]), its valence band (VB) edge usually lies at $+1.4$ V vs. NHE, being its applicability for photo-oxidative reactions (e.g., degradation of emerging contaminants [13]) limited to few scenarios. In an aqueous system, although possible the reduction of dissolved oxygen into H$_2$O$_2$ or O$_2^{\bullet-}$, the latter reduced into further H$_2$O$_2$ (see R1-R3), the oxidation of water into H$_2$O$_2$ or HO$^{\bullet}$ (R4 and R5, respectively) are thermodynamically unviable, whereas the O$_2$ evolution (R6) is kinetically unfavoured as it requires 4 electrons. For these reasons, with illuminated g-CN: *i)* in order to observe considerable H$_2$O$_2$ photo-production rates, a hole scavenger (e.g., methanol, R7) is needed to avoid the fast electron-hole recombination and the H$_2$O$_2$ oxidation by the photogenerated holes, respectively, *ii)* the contribution of holes and HO$_2^{\bullet}$/O$_2^{\bullet-}$ towards the overall degradation of pollutants is considerably more important than that coming from HO$^{\bullet}$ alone [14].

$$O_2 + 2\ H^+ + 2\ e^- \rightarrow H_2O_2;\ E° = 0.68\ V\ vs.\ NHE \qquad (R1)$$

$$O_2 + e^- \rightarrow O_2^{\bullet-};\ E° = \text{-}0.33\ V\ vs.\ NHE \qquad (R2)$$

$$HO_2^{\bullet} + H^+ + e^- \rightarrow H_2O_2;\ E° = 1.44\ V\ vs.\ NHE \qquad (R3)$$

$$H_2O_2 + 2\ H^+ + 2\ e^- \rightarrow 2\ H_2O;\ E° = 1.78\ V\ vs.\ NHE \qquad (R4)$$

$$HO^{\bullet} + H^+ + e^- \rightarrow H_2O;\ E° = 2.80\ V\ vs.\ NHE \qquad (R5)$$

$$O_2 + 4\ H^+ + 4\ e^- \rightarrow 2\ H_2O;\ E° = 1.23\ V\ vs.\ NHE \qquad (R6)$$

$$^{\bullet}CH_2OH + H^+ + e^- \rightarrow CH_3OH;\ E° = 1.2\ V\ vs.\ NHE \qquad (R7)$$
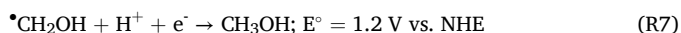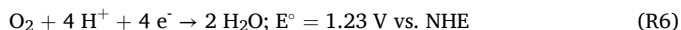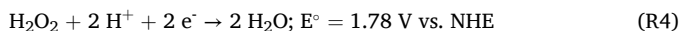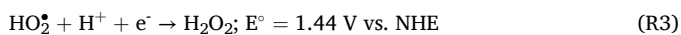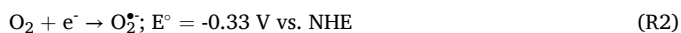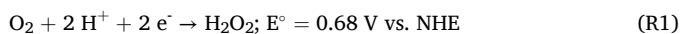
Due to its low band gap energy (E$_g$, $\approx$ 2.6 eV), most studies analysing the photocatalytic activity of g-CN focus on decreasing the E$_g$ at all costs in order to drive photochemical reactions within the visible spectrum range [15–17]. For example, for the sake of obtaining considerable H$_2$O$_2$ photo-production rates (ca. 2 mM h^{-1}), sophisticated synthesis (e.g., applying several calcination steps —with temperatures ca. 600°C— and adding dopants) and favourable operational conditions (e.g., employing high concentrations of hole scavengers, use of intense Xe lamps, and O$_2$ saturated atmospheres) are required [18–20]. Actual ultraviolet (UV) light emission diodes (LED) consume low energy, as well as the electrical current is tending to be completely fossil-fuel free in the near future [21]. In this perspective, a trade-off can be reached by preparing carbon nitride materials at lower temperatures within 400 – 500 °C (this is, employing the melem oligomers instead of melon or "g-C$_3$N$_4$") and simply applying irradiations in the UV range. Furthermore, the idea of developing a photocatalyst to be efficient under the visible region does not necessarily mean that it will also exhibit good performances within the ultraviolet one.

Despite the advantages of UV lamps over visible ones (or sunlight, not always present), there is a lack of works applying them to perform photocatalytic reactions with g-CN-based materials. The same applies for low polymerisation carbon nitride compounds: although there is an increasing number of publications exploring melem-based photocatalytic activities (usually higher than that of g-C$_3$N$_4$), the prevailing focus in the literature is placed on the polymer melon, overlooking the diverse carbon nitride materials with varying degrees of polymerization

[6,22,23]. These issues together could be particularly relevant either for green H$_2$O$_2$ production (its photolysis is low if UVA light, $\lambda_{max} \approx$ 360 nm, is used [24]) or emerging contaminants degradation from water [7].

Since visible light/g-C$_3$N$_4$ has been mostly employed based on tradition rather than optimisation of a specific final target, in this work, we have thoroughly compared the photocatalytic activity, under UVA and visible light, of melam, melem and melon towards H$_2$O$_2$ generation and phenol (proposed as model emerging contaminant) oxidation. Continuing with the line of unquestionable traditions, we have also checked if covering the crucibles is beneficial or not, which is stated to reduce the melamine sublimation and contain the generated NH$_3$ in the vessel, influencing the final product [25,26]. In order to correlate the generated data (i.e., the results of both the physico-chemical characterization and the photochemical behaviour from all the synthesized materials), Principal Component Analysis (PCA) was employed as a powerful chemometric tool to highlight correlations among the explored variables, obtaining some general and synoptic conclusions. In spite of its simplicity, there are very few works employing the PCA to improve the materials synthesis and / or determine the dominant factors influencing the catalytic process being studied [27–29]. Our work intends to analyse if complex synthesis process for g-CN preparation is as needed as stated in the literature.

2. Materials and methods

2.1. Reagents

Melamine, NaOH, NaH$_2$PO$_4$, Na$_2$HPO$_4$, phenol, sodium hexane sulfonate, horseradish peroxidase, and 4-aminoantipyrine were purchased from Sigma-Aldrich. H$_2$O$_2$ 33 % V/V, HClO$_4$ 70 %, H$_3$PO$_4$ 85 %, and UHPLC grade CH$_3$OH and CH$_3$CN were obtained from VWR Chemicals.

2.2. Carbon nitride synthesis

Different g-CN were synthesised by thermal polycondensation of melamine as widely reported [18,30]. 2 g of melamine were introduced into alumina crucibles (with and without an aluminium foil cover) and placed inside a horizontal tubular oven (Lenton LHC 12/750). A gradient temperature of 5 °C min^{-1} was employed to reach the desired temperature: 350, 425, 500, 575 and 650 °C, respectively, which was subsequently kept constant for 2 h. The materials were then allowed to cool naturally to room temperature in the oven. During the whole process, N$_2$ current was flown through the oven to ensure anoxic conditions. The obtained solids were grounded with a mortar until a fine powder was obtained. Afterwards, these were washed with water and methanol. The obtained semiconductors were named according to the *plateu* temperature, T, of synthesis as g-CN-T, and, for the series where aluminium foil cover was used, g-CN-T-Al. For example, the photocatalyst resulting from melamine placed in the covered crucible and calcinated at 500 °C was named as g-CN-500-Al.

2.3. Materials characterisation

Unreacted melamine content was determined by high performance liquid chromatography (described in **Section 2.5**). For that, aqueous suspensions of g-CN-T and g-CN-T-Al (without the washings with water and methanol) were left overnight under agitation and afterwards filtered, measuring the dissolved melamine from the washing solution.

The optical and electronic properties were characterised by UV–vis diffuse-reflectance spectroscopy (Varian Cary 5000 UV-Vis-NIR), fluorescence spectroscopy (Varian Cary Eclipse) and cyclic voltammetry (potentiostat PGSTAT12, Autolab), respectively. Regarding the latter, drops of g-CN-T(-Al) suspension were deposited on glassy carbon conductive electrodes and subsequently dried at 80 °C in an oven, resulting in a thin layer of ca. 2 mg of material on each electrode (surface

6.25 cm^2). A conventional three-electrode cell was employed: the counter electrode was a Pt sheet, the reference electrode was Ag/AgCl/KCl (3 M), and the electrolytic solution was NaClO$_4$ 0.1 M in acetonitrile; nitrogen purging was always applied to ensure negligible O$_2$ concentrations. The scan rate was 0.5 V s^{-1} and the range, $-1.75 - 2.5$ V.

C, N, H and O content were measured by elemental analysis (Thermo Fisher CHNS-O analyser, Flash EA 1112 series); the procedure consisted of mixing 2.5 mg of each sample with an excess of the corresponding catalyst - V$_2$O$_5$ - and placing it into a tin crucible.

The paramagnetic character was determined by solid-state electron paramagnetic resonance (EPR). The spectra were recorded on a Bruker EMX spectrometer working in X–band (9.5 GHz), equipped with finger dewar; all measurements were performed at 77 K with 1 mW microwave power, 0.1 mT modulation amplitude and 100 kHz modulation frequency [31]. Evaluation of the number of spin/g was performed using the Xenon software (Bruker), taking into account the mass of the sample. Photoinduced EPR spectra were recorded irradiating the samples *in situ* using a 500 W Hg(Xe) lamp (Newport Instruments) equipped with a water filter to cut the IR emission and a cut-off filter at 420 nm.

Functional groups and molecular structures were investigated through Fourier transform infrared spectroscopy (FTIR, Perkin Elmer Spectrum Two), Raman spectroscopy (Bruker Vertex 70 spectrometer, equipped with the RAMII accessory, excitation at 1064 nm), and X-ray diffraction (XRD, Panalytical Empyrean diffractometer, equipped with a CuKα radiation and a PIXCel3D detector).

Surface area and particle sizes/shapes were not characterised because these data have been previously provided in similar studies [7, 8], usually being stated that textural/surface properties are not detrimental factors explaining g-CN-T photocatalytic activities compared to those from chemical composition or electronic properties [22,32]. Moreover, microscopic analysis gives information hardly used in the PCA (*vide infra*) employed to highlight the correlations among all experimental variables measured.

2.4. Photocatalytic activity

The photocatalytic activity of the obtained materials was studied in terms of its reducing capacity (by means of H$_2$O$_2$ photogeneration, employing CH$_3$OH 3 M as hole scavenger), and also by their oxidative performance (by means of phenol 100 µM degradation). The experiments were carried out in ultra-pure water at non-adjusted pH (ca. 6.0) containing 1.65 g L^{-1} of synthesised g-CN-T(-Al). The employed working conditions (CH$_3$OH concentration and photocatalyst amount) were selected based on Design of Experiment – response surface methodology preliminary experiments (see Supporting Information, **Text S1**). In all cases, closed cylindrical Pyrex cells (4.0 cm diameter and 2.5 cm height, cut-off at 295 nm) containing 5 mL of the testing suspension were employed and continuously magnetically stirred. Irradiations were performed employing visible light (TOT Electric LED, 69 lux) or UVA light (Philips BLB fluorescent lamp, 20 W m^{-2}), whose normalised emission spectra are reported in Figure S2. Previous irradiation, g-CN-T (-Al) were exfoliated by sonicating (Branson 2800 sonicator) a 2.5 g L^{-1} suspension in ultra-pure water for 30 min. The irradiated Pyrex cells were retired at different time intervals, and suspensions filtered through 0.45 µm hydrophilic PTFE membranes (Millipore Millex-LCR) before the analysis. When needed, anaerobic conditions were obtained by bubbling N$_2$ gas in the reactor for 15 min before the irradiation; caps with gum-septum were employed to avoid O$_2$ diffusion in the cells during the nitrogen purging.

2.4.1. Blank experiments

Blanks consisted of: phenol adsorption on g-CN-T(-Al) materials, phenol photodegradation by UVA and visible light (alone and in presence of H$_2$O$_2$ 1 mM, respectively), and H$_2$O$_2$ photolysis by UVA and visible light.

The adsorption of phenol on g-CN-T-(Al) materials was negligible in all cases ($<$5 % in 3 h). Phenol photolytic decomposition was also negligible after 3 h of irradiation with UVA and visible light, respectively; noteworthy, in presence of H$_2$O$_2$ 1 mM (simulating the H$_2$O$_2$ generated by g-CN), 20 % phenol degradation after 3 h was observed (only with UVA light, being imperceptible with visible light). Finally, blank control irradiating H$_2$O$_2$ 1 mM solution indicated that 20 % of H$_2$O$_2$ photolysed under UVA in 3 h, while no photolysis was observed under visible light.

2.5. Analytical measurements

H$_2$O$_2$ concentration was measured by colorimetric method, adapted from [33], employing a solution containing 0.234 % m/V of phenol, 0.10 % m/V of 4-aminoantipyrine, 0.0010 % m/V of peroxidase, dissolved in buffer phosphate pH 7.0, and measuring the resulting absorbance at 505 nm with a spectrophotometer Varian Cary 100 Scan.

Phenol degradation was determined with HPLC-UV/vis (YL9300 HPLC System, Lichrospher R100 RP-18 5 µm column) coupled to UV/vis detector ($\lambda = 220$ nm) employing 1 mL min^{-1} mobile phase consisting of H$_3$PO$_4$ 5 mM : CH$_3$OH, 80:20 (% V/V). The same instrument was employed for melamine determination (mentioned in **Section 2.3**), consisting of a mobile phase of 95 % V/V of 0.01 M sodium hexane sulfonate and 0.014 M H$_3$PO$_4$ (both dissolved in water), and 5 % V/V of acetonitrile [34].

When needed, H$_2$ generation was measured by sampling 2.5 mL of headspace (septum caps were employed in this case) after irradiation and analysed through an Agilent 490 Micro GC gas chromatograph equipped with a Molsieve 5Å column for H$_2$ analysis, as described in a previous work [35].

2.6. Multivariate analysis

The principal component analysis (PCA) was carried out to correlate the results of the materials' characterizations with those from irradiation experiments, and was obtained through the free and user-friendly software CAT (Chemometric Agile Tool) [36]. The employed dataset is shown in Table S3.

3. Results and discussion

3.1. Characterisation results

3.1.1. Synthesis yields and content of unreacted melamine

As shown in Table S3, the mass loss significantly incremented when increasing the temperature above 350 °C, being of 11 % in the latter, but ca. 80 % for those prepared in the range 425 – 575 °C. At T $>$ 600 °C the g-CN decomposition into HCN, NH$_3$ and C$_2$N$_2$ becomes significant [8], explaining the extremely low yield of 1 % obtained at 650 °C. As expected, when covering the crucibles with the aluminium foil, the mass loss was drastically reduced for each of the applied temperatures, in line with other works stating a lower melamine loss by sublimation [37]. Even in the extreme case of 650 °C (g-CN-650-Al), the synthesis yield was of 28 %. Therefore, the synthesis in the covered vessel must reduce the g-CN thermal decomposition, in line with the literature [26].

The content of unreacted melamine was also in line with the applied temperature (i.e., polymerisation degree). The former was only significative in the materials prepared at 350 °C, g-CN-350 and g-CN-350-Al, being of 1 and 26 % m/m, respectively. g-CN-425(-Al) only contained approximately 0.1 % m/m of melamine. Above 500 °C, the melamine content was negligible.

3.1.2. Optical and electronic properties

In both series, g-CN-T and g-CN-T-Al, reflectance increases at higher wavelengths in correlation with the chosen polycondensation temperature, observed in the colour of the respective solids (from white at 350 °C, to pale yellow at 500 °C, and ending with reddish colour at 650 °C).

This red-shift in the reflectance spectra is related to the degree of conjugation increment in the synthesized structure as a consequence of a higher polymerization degree [5,7]. Diffuse reflectance spectra of the synthesised materials are shown in Fig. 1A and B.

To calculate the corresponding direct and indirect transition band gap energies, Kubelka-Munk function (Eq. 1) was employed, where $F(R_\infty)$ is the reflectance of an infinitely thick solid, h the Planck constant (eV s), ν the photon's frequency (s^{-1}), γ a factor related to the transition (considering only allowed transitions, $\gamma = 1/2$ and $\gamma = 2$ for direct and indirect transitions, respectively), E_g the band gap energy (eV), and B a proportionality constant [38]. Therefore, by normalising the direct reflectance value from the respective g-CN and elevating it to ½ and 2 depending on direct and indirect transitions, respectively (see Figures S3 and S4), one can calculate the E_g values of each transition.

$$(F(R_\infty)h\nu)^{1/\gamma} = B(h\nu - E_g) \tag{1}$$

Obtained E_g values for the materials prepared at 575 and 650 °C (ca. 2.2 – 1.6 eV) are significantly below from those published in similar works (ca. 2.65 eV as previously mentioned [7]). This is because the E_g value depends on the chosen γ; assuming a direct transition where might be unlikely, will give as a result unrealistic E_g values [30]. In this sense, fluorescence emission could be more precise towards direct transitions and cyclic voltammetry for indirect ones (although the latter is also sensitive to trap states).

Regarding the fluorescence analysis, when shifting from g-CN-350 (-Al) to g-CN-650(-Al), emission maxima explored red-shift from 375 till 475 nm, detecting an inflection point ca. 425 nm (see Fig. 1C and D for g-CN-T and g-CN-T-Al, respectively). This inflection point indicates the transformation from lower molecular weight carbon nitrides (melam and melem) into a major product with higher degree of electronic delocalisation (melon). Fluorescence excitation-emission matrices of each photocatalyst are shown in Figure S5.

Emission maxima of g-CN-350 and g-CN-350-Al were $\lambda_{ex} < 250$ nm and $\lambda_{em} = 370$ nm, in line with the presence of aforementioned melamine-like compounds (the reported fluorescence maximum of melamine is, in fact, $\lambda_{ex} < 250$ nm and $\lambda_{em} = 375$ nm [39]) and the measured content of unreacted-melamine on unwashed g-CN-350(-Al) (mentioned in **Section 3.1.1**). The photocatalysts synthesised with T > 500 °C had emission maxima above 440 nm (≈ 2.8 eV) in agreement with the reported band gaps for g-CN. For instance, g-CN-500-Al, g-CN-575-Al and g-CN-650-Al, had their fluorescence maxima emission at 440, 465 and 475 nm, respectively. Analogous trend was obtained for the series without the Al foil, except that for g-CN-650, where negligible fluorescence was observed.

Differently from diffuse reflectance, fluorescence emission is linked only to direct allowed transitions [32]. The absence of fluorescence in g-CN-650 suggests predominance of indirect transitions (common for doped photocatalyst [30]). Since fluorescence intensity decays with increasing calcination temperature (see Table S3 and Figure S5), being negligible for g-CN-650, plausible p-doping product of increasing C-content should be obtained at higher polycondensation temperatures. Therefore, g-CN-650 must have a content of carbon higher than those prepared with lower temperatures as well as localised orbitals should also be present close to VB (confirmed by C:N elemental analysis and solid state EPR analysis, respectively, described in the following section).

To gain further insights into the electronic properties of g-CN-T(-Al) materials, cyclic voltammetry measurements were performed, calculating the related Density of States (DoS) based on Eq. 2, where p (g^{-1} V^{-1}) is the density of monoelectronic states in the potential range, dE (V), m (g) the deposited mass of photocatalyst on the electrode, e the electron charge (1.60×10^{-19} C), i (A) the measured current, s (V s^{-1}) the scan rate.

$$DoS = \int p(E)dE = \frac{1}{me}\int \frac{i}{s}dE \tag{2}$$

By considering levels close to the valence and conduction bands (VB and CB, respectively), the DoS usually increases exponentially because of the presence of localized states, and this increment becomes more pronounced when the applied potential crosses the VB/CB edges [40]. Nevertheless, hardly can a sharp discontinuity be found when applied potential crossed band edges. This phenomenon could be related to Fermi level pinning effect: at the band edges the charge accumulated into the semiconductor space charge layer becomes of the same order of magnitude of that stored in the Helmholtz layer [41,42]. Thus, the detection of CB and VB edges becomes extremely challenging and speculative. Nonetheless, plots of E vs. DoS (see Figures S6 and S7 for g-CN-T and g-CN-T-Al, respectively) contain valuable information, as they represent an electronic fingerprint of the particular material.

In line with the fluorescence results, localised states were mostly evidenced for g-CN-650. Interestingly, DoS results did not follow a trend with calcination temperature, furthermore they differed between the series with and without the Al-foil covering. Regarding g-CN-T series, the DoS reached the highest values at 2.5 and -1.75 V, respectively, with those prepared at 350 or 425 °C, and not with 650 °C, which was counterintuitive. Therefore, to better understand the electronic properties of the prepared photocatalysts, we focused on the DoS at particular potential values, at which reactions of interest can be promoted. Here the focus was placed in those reactions relevant towards H_2O_2 photo-production. Consequently, regarding the CB's e⁻, the reactions involved in the H_2O_2 formation were R1 to R3, and the counterproductive reaction of its reduction into water (R4). For the VB's h⁺ we considered the oxidation of: the probe (CH_3OH, R7), H_2O_2 into $HO_2^\bullet$ and O_2, respectively, $O_2^{\bullet-}$ into O_2, and H_2O into H_2O_2. The formation of $HO^\bullet$ (R5) and O_2 (R6) were considered irrelevant for the reasons given in the introduction section.

DoS was, therefore, integrated in the intervals of potential of the reactions of interest $+0.4$ V in case of anodic current and -0.4 V for cathodic ones (considering the correction for pH and the AgCl/Ag electrode). For example, for the reduction of O_2 into H_2O_2, the standard redox potential is 0.68 V, which at pH = 6.0 becomes 0.50 V, and with respect to the reference electrode translates to 0.28 V. Therefore, the CB's DoS was integrated from 0.28 V up to -0.12 V. These intervals should contain the electronic states with the largest probability of promoting the reaction of interest. In the case of $O_2/O_2^{\bullet-}$ we considered the reported E = -0.16 V vs. NHE at pH 7 (= -0.38 V vs. AgCl/Ag) [43]. Results are shown in Fig. 1E-H.

Starting with series without covering the crucible with Al (Fig. 1E), g-CN-425 was the one with the highest DoS for every reductive reaction considered for the calculations. In particular for O_2 reduction into $O_2^{\bullet-}$ (with the highest values), the DoS were of 9.4×10^{14} g^{-1}, followed by g-CN-650 (8.3×10^{14} g^{-1}) > g-CN-500 (7.1×10^{14} g^{-1}) > g-CN-575 (5.8×10^{14} g^{-1}) > g-CN-350 (4.9×10^{14} g^{-1}). Regarding the oxidative reactions (Fig. 1G), besides the DoS obtained at the redox potential of methanol (where no significative differences were observed between the different calcination temperatures), g-CN-425 exhibited the greatest DoS for water oxidation into H_2O_2 as well as for H_2O_2 oxidation into $HO_2^\bullet$. Interestingly, g-CN-650 was the one with the highest DoS at the potentials for H_2O_2 oxidation into O_2 and $O_2^{\bullet-}$ into O_2.

For the series prepared by covering the crucibles with Al foil, the trend was completely different; without considering g-CN-350-Al (an outlier in both anodic and cathodic measurements, probably due to the presence of melamine-like compounds), the ones with the highest DoS for reductive and oxidative reactions were the materials prepared at 500 and 575 °C (see Fig. 1F and H).

Therefore, differently from diffuse reflectance and fluorescence analysis (where values changed accordingly with calcination temperature) no correlation was observed with cyclic voltammetry analysis and calcination temperature. This might indicate that a change in E_g does not necessarily mean to be synonymous of change in reduction/oxidation efficiency.
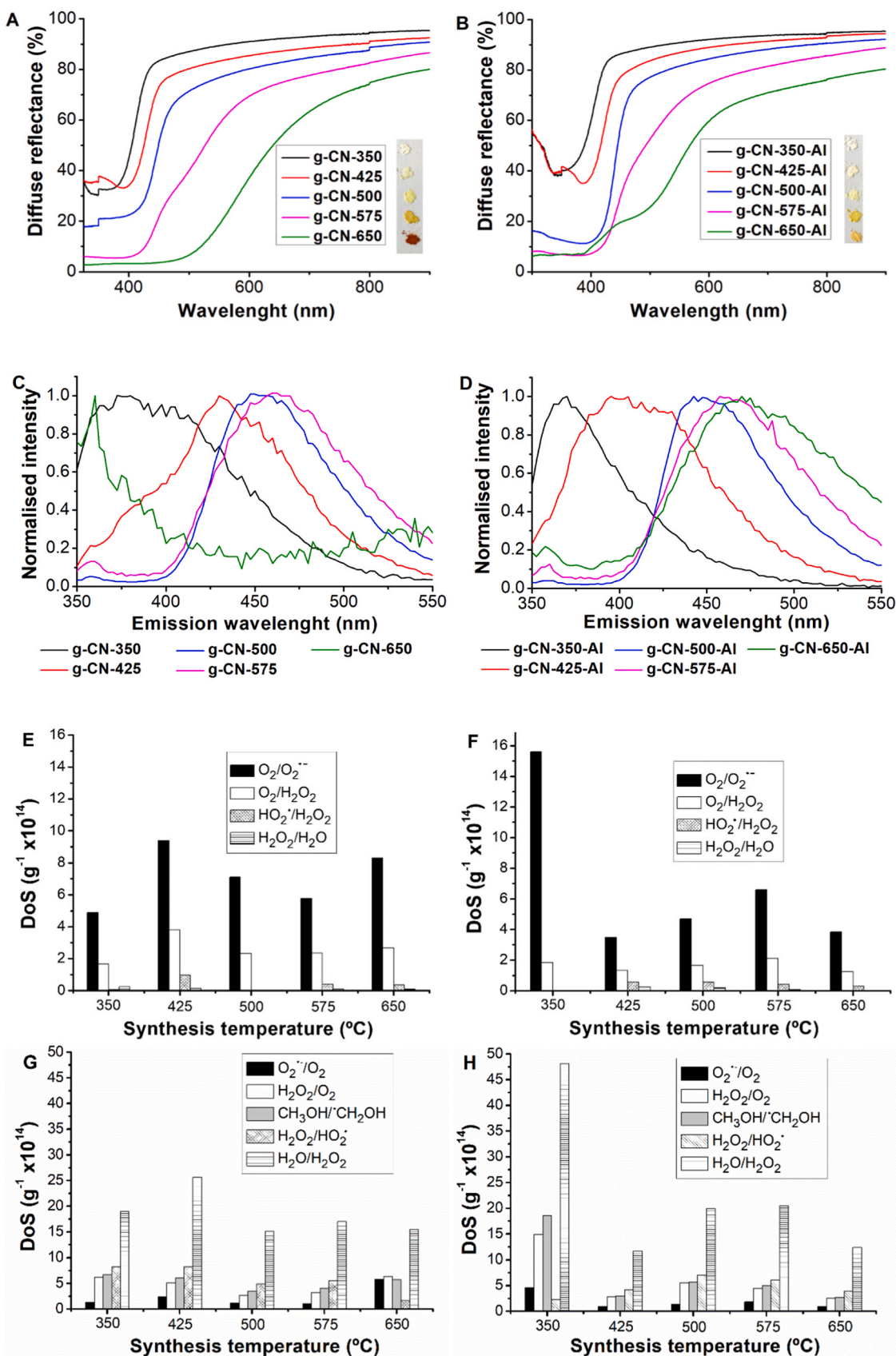
Fig. 1. Diffuse reflectance spectra of the different g-CN synthesized at different temperatures (photograph as an inset): A) g-CN-T and B) g-CN-T-Al. Normalised fluorescence emission maxima (λ_{exc} = 320 nm): C) g-CN-T and D) g-CN-T-Al. DoS from cathodic current (reductive reactions): E) g-CN-T and F) g-CN-T-Al. DoS from anodic current (oxidative reactions): G) g-CN-T and H) g-CN-T-Al.

3.1.3. Chemical properties

The ideal graphitic carbon nitride has a C:N ratio of 0.75. From our materials, this was almost reached only by g-CN-650, which displayed a C:N = 0.74 (Fig. 2A). Carbon nitride calcinated at $575°C \geq T \geq 350$ °C resulted in $0.69 \geq C:N \geq 0.62$, representing a lower degree of polymerisation and presence of smaller size oligomer and chain terminations. The same trend was observed for g-CN-T-Al (Fig. 2B); these, however, were lower if compared to their analogous prepared without covering the crucible (e.g, C:N of g-CN-425-Al was 0.620, whereas for g-CN-425 was 0.644), indicating that the aluminium foil reduces the polymerisation degree. In addition, in both series (with and without the aluminium cover), the H:C ratio is reduced with increasing temperatures. These results are in line with the ones observed from diffuse reflectance and fluorescence, as well as with the vast literature on the matter [6]. The oxygen content was negligible in all cases (<0.5 % m/m), in consonance with the anoxic conditions employed in the tubular furnace used for the synthesis.

Spin counting performed on the EPR signals in the dark (Figure S8A) indicated that higher condensation temperatures (namely 575 and 600 °C) result in a markedly higher number of spins, suggesting that higher temperatures of synthesis determine a higher concentration of defective radical species ($S = \frac{1}{2}$) in the material [44,45]. Except for g-CN-650 and g-CN-650-Al, where the latter exhibited greater spin counting, the Al cover reduced the number of spins/g for all applied temperatures. The discrepancy of 650 °C can be explained by the fact that at this extreme temperature, g-CN-650 must be partially degraded (as suggested in Section 3.1.1), affecting the π-conjugated system, reducing the spin/g number [46]. On the other hand, Figure S8B and C show the peak-to-peak intensity of the EPR signals as a function of irradiation

time (from 0 to 10 minutes) under visible light at 77 K. In line with the dark measurements, higher polymerisation led to a stronger photo-response linked to an increase in the concentration of radicals (i. e., unpaired electrons) in the material upon irradiation, in line with previous literature reports [47,48].

The chemical structure evolution with temperature were analysed by FTIR, FT-Raman and XRD. FTIR results shows (Fig. 3A and D) analogous trends to those reported in previous studies with increasing temperatures: i) stretching and deformation modes of -NH$_2$ groups (3300–3470 cm^{-1}) decrease, ii) lower absorption of the s-triazine ring mode peak of 800 cm^{-1} presented a marked peak on melamine and low temperatures g-CN, iii) broadening in the ν(C-N) region around 1320 cm^{-1}; and iv) absorption increment around 1400 – 1600 cm^{-1} signals [49,50]. Therefore, signals below 800 cm^{-1} disappear with increasing temperature, whereas those at 1300 – 1600 cm^{-1} notably increase. However, this trend was not observed when comparing g-CN-650 with g-CN-650-Al, the first with broaden signals and the last with marked ones, indicating that the calcination in the open crucibles leads to more amorphous materials and with the closed ones to more crystalline ones. This was also evidenced by Raman spectroscopy (Fig. 3B and E), where clear signals were observed for g-CN-650-Al whereas a smooth spectrum was obtained for g-CN-650 with no clear Raman peaks. In fact, g-CN-650-Al could be considered an outlier itself, as the crystallinity of the latter seems to be even higher than that obtained with lower temperatures (e.g., g-CN-575-Al). The complex issues governing the crystallinity of gCN are related to temperature and NH$_3$ partial pressure, as previously reported [26].

The higher crystallinity of g-CN-650-Al was also evidenced by XRD analysis (Fig. 3C and F). Except for this particular case, the same trend as with EPR, FTIR or Raman was observed, indicating increasing polymerisation with applied temperature and absence of aluminium foil cover, thus, detecting sharp and multiple diffraction peaks at low synthesis temperatures (or closed crucibles for a same condition), which were diminished and broaden to a major signal with increasing synthesis temperatures. These results are in line with the extended literature on the matter [6,7,32,50–53], observing some characteristic diffraction peaks such as: $2\theta = 14.2°$ and $26.0°$ of melam, $2\theta = 12.5°$ and $27.7°$ of melem, and two single wide diffraction peaks corresponding to melon at $2\theta = 12 – 15°$ (in-plane structural motif) and $25 – 30°$ ((002) stacking of polymeric sheets), which evidence the latter's long-range order across the plane and turbostratic disorder in the stacking direction.

Based on the above mentioned statements, we can classify the obtained g-CN materials as following: g-CN-350-Al, oligomeric melam; g-CN-350, melam-melem oligomer adducts; g-CN-425-Al, oligomeric melem; g-CN-425 and g-CN-500-Al, melem-melon oligomer adducts; g-CN-500 and g-CN-575(-Al) melon; and g-CN-650(-Al) melon-g-C$_3$N$_4$.

3.2. H$_2$O$_2$ photo-production performance

The following subsections show the obtained H$_2$O$_2$ photogeneration profiles under UVA and visible light, respectively, when irradiating 1.65 g L^{-1} of the aforementioned materials in presence of CH$_3$OH 3 M as hole scavenger.

3.2.1. UVA light irradiation

As observed in Fig. 4A and B, a monotonic increasing behaviour is observed in all cases, indicating scarce H$_2$O$_2$ degradation by oxidation from VB holes (expected due to the excess of CH$_3$OH) and compensating the low, but present, H$_2$O$_2$ direct photolysis (see Section 2.4.1).

Overall, for those prepared in the open crucibles, the H$_2$O$_2$ photo-production followed the order g-CN-500 $\geq$ g-CN-425 > g-CN-575 > g-CN-350 >> g-CN-650, whereas for those prepared in the closed crucibles the differences were more marked, being the decreasing order as following: g-CN-425-Al >> g-CN-500-Al > g-CN-575-Al > g-CN-650-Al >> g-CN-350-Al. Therefore, as observed with DoS values, a reduction of the E$_g$ (i.e., employing a higher calcination temperature, thus tending to
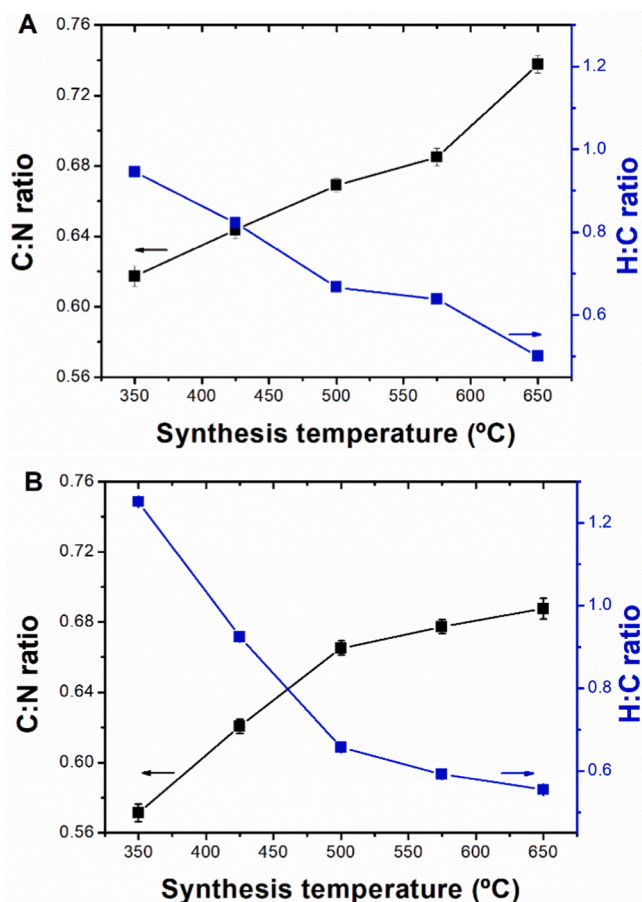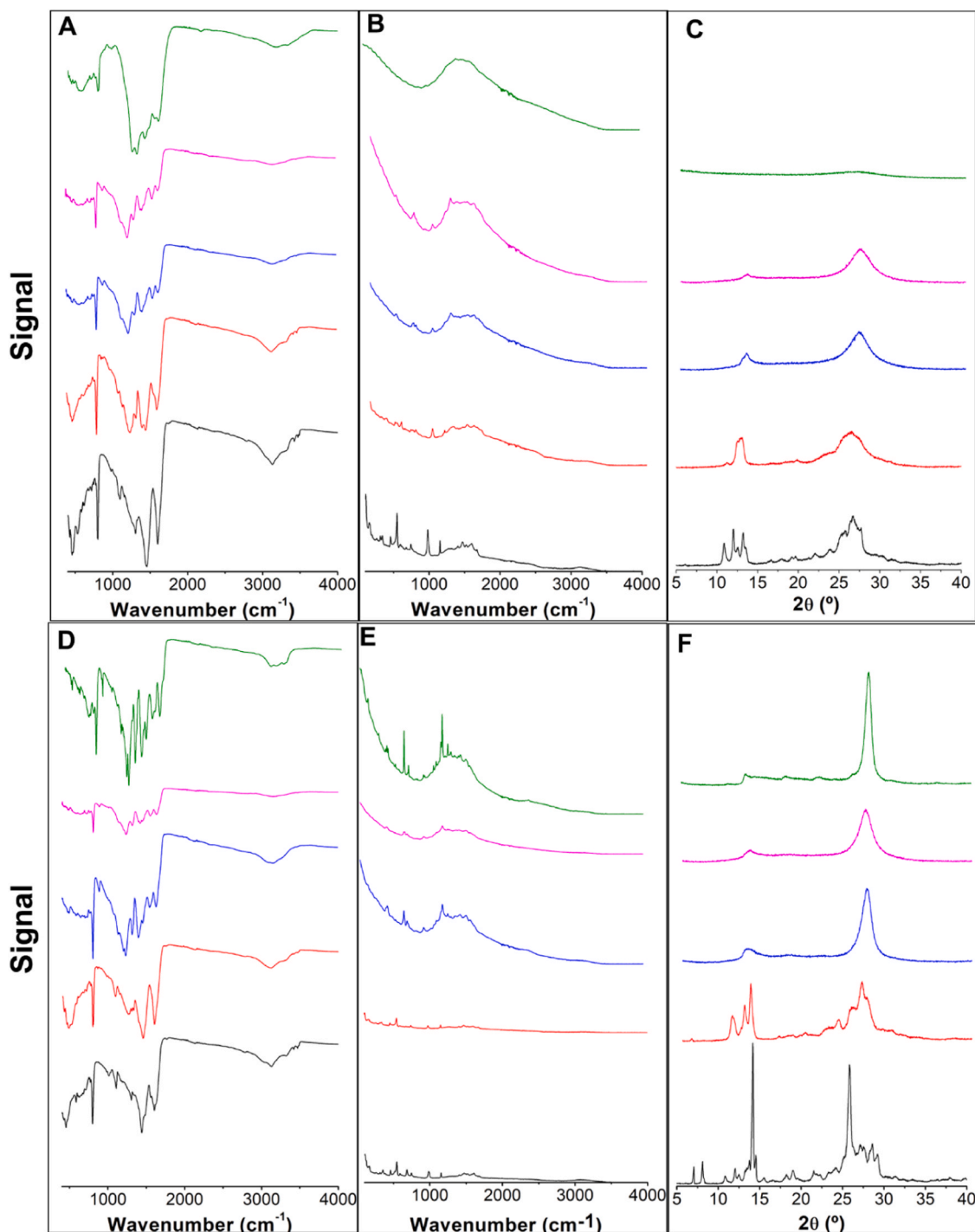

Fig. 2. C:N and H:C ratios of the synthesised semiconductors according to the applied temperature: A) g-CN-T, and B) g-CN-T-Al.

Fig. 3. FTIR, FT-Raman and XRD results for g-CN-T (A, B and C, respectively) and g-CN-T-Al (D, E and F, respectively). Synthesis temperatures: 350 ℃ (black), 425 ℃ (red), 500 ℃ (blue), 575 ℃ (magenta), and 650 ℃ (green).

C:N = 0.75) is not linked to higher O_2 reductive character.

The obtained results indicated that oligomeric melem materials were the ones exhibiting the highest photocatalytic activities, g-CN-425-Al producing after 3 h an outstanding concentration of 6.0±0.2 mM of H_2O_2, being the most efficient one from all the synthesised photocatalysts (Fig. 4B).

If compared with other works employing similar hole scavenger concentrations, g-CN-425-Al (melem) led to comparable, or even higher, H_2O_2 photo-production rates than g-CN based materials prepared with more complex procedures [18,20,54–56]. Furthermore, g-CN-650 (the closest to ideal g-C_3N_4) was the photocatalyst with the lowest H_2O_2

photoproduction from all the prepared semiconductors, with barely 0.1 mM H_2O_2 in 3 h (Fig. 4A). This value was even below that of g-CN-350-Al (oligomeric melam), the latter producing 0.8 mM of H_2O_2 in 3 h. The reason of the utterly low H_2O_2 production by g-CN-650 could be related to the plausible oxidation of H_2O_2 by photogenerated holes. In fact, g-CN-650 was the one with the highest DoS at H_2O_2/O_2 oxidation potential (see Fig. 1G).

Finally, since studying the stability of g-CN is usually neglected, the H_2O_2 photoproduction was measured for the g-CN-T(-Al) after one year of preparation and after a pre-irradiation with UVA light for 24 h. Results indicated that, in both cases, the photocatalytic activity was
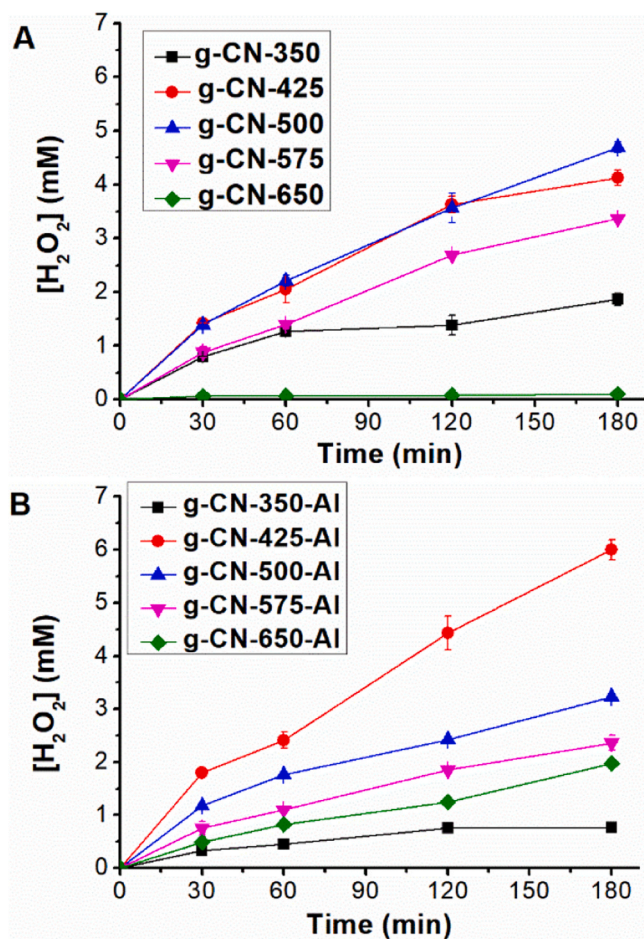
Fig. 4. H_2O_2 photogeneration under ultraviolet-A light by, A) g-CN-T and B) g-CN-T-Al. Conditions: amount of g-CN-T(-Al) = 1.65 g L^{-1}, [CH_3OH] = 3 M, initial pH = 6.0.

Fig. 5. H_2O_2 photogeneration under visible light, by A) g-CN-T; B) g-CN-T-Al. Conditions: amount of g-CN-T(-Al) = 1.65 g L^{-1}, [CH_3OH] = 3 M, initial pH = 6.0.

analogous to that represented in Fig. 4, which are in line with other works stating that melem oligomers are as stable as melon polymers [22], or that only when significative $HO^{\bullet}$ is formed g-CN is oxidised [57], which is not the case here.

3.2.2. Visible light irradiation

By using visible irradiation (400 – 800 nm) the population of excited electrons at g-CN CB diminishes compared to UVA irradiation (340 – 400 nm). Therefore, it should be expected a better correlation between E_g values with measured H_2O_2 photogeneration. Indeed, for fixed temperature but changing the series, g-CN-T vs. g-CN-T-Al, the H_2O_2 formation was higher for those prepared in the open crucibles (see Fig. 5A and B, respectively), in line with their lower E_g (see Table S3). For instance, g-CN-500 (E_g = 2.79 eV) lead to ca. 300 µM concentration of H_2O_2 at 3 h, whereas g-CN-500-Al (E_g = 2.82 eV) was of 175 µM in the same period. Noteworthy, when comparing the materials from the same series, the relationship of H_2O_2 photoproduction was not strictly in line with E_g values (i.e., synthesis temperature). H_2O_2 production rate by g-CN-500, g-CN-575 and g-CN-650 was similar, with an average 100±25 µM h^{-1}, subsequently followed by g-CN-425 (ca. 60 µM h^{-1}). Evidently, with g-CN-350 (E_g = 3.35 eV), the H_2O_2 generation was negligible, reaching 15 µM after 3 h of irradiation. Regarding the series with Al cover, g-CN-425-Al and g-CN-500-Al produced 160 µM of H_2O_2 in 3 h, whereas g-CN-575-Al and g-CN-650-Al with 85 µM in the same period. Also in this case the material prepared at the lowest temperature (g-CN-350-Al) was ineffective in the synthesis of H_2O_2.

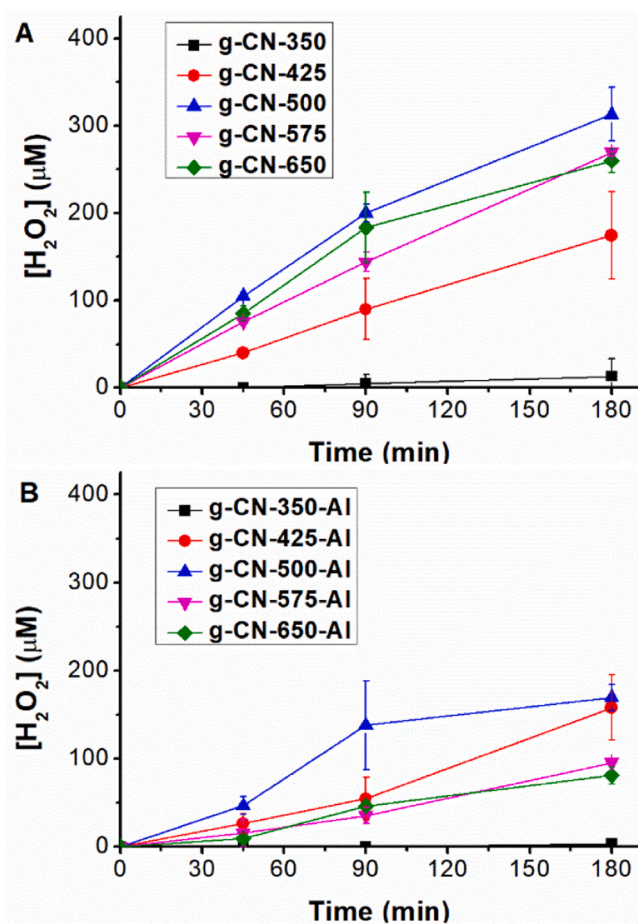When confronting the performance of g-CN-650 under UVA and

visible light (Figs. 4A and 5A, respectively), lower H_2O_2 final concentrations were reached with the former (103 µM after 3 h of UVA irradiation vs. 260 µM in the same period with visible light). This is in line with the hypothesis of a stronger oxidative VB by g-CN-650 compared to its less polymerised analogues, as when higher energetical photons are employed, the photocatalytic oxidation of H_2O_2 into O_2 must occur, explaining its lower generation when employing UVA light compared to visible light.

Based on the above mentioned results, except for those synthesised at 350 °C (with a clear lack of ability for O_2 reduction with visible light), those prepared within 425 and 650 °C have comparable H_2O_2 production rates. The still good performance of visible/g-CN-425(-Al) was, at least, unexpected due to its low degree of polymerisation. As reported by B. V. Lotsch and co-workers (2015), since the melem oligomer exhibits lower absorption within visible region than melon or g-C_3N_4 (see Fig. 1A-B), its good photocatalytic activity should not be related to a higher collection of more photons, but rather because of the improved either charge separation or interfacial charge transfer [22].

3.3. Phenol oxidation performance

3.3.1. UVA light irradiation

Phenol 100 µM degradation was firstly studied under UVA irradiation. Similarly as the H_2O_2 photo-production in presence of methanol, g-CN-425 and g-CN-425-Al exhibited the best performances, exhibiting kinetic rate constants of 4.5×10^{-2} and 3.9×10^{-2} min^{-1}, respectively (see Fig. 6A and B). These results are also comparable (or even faster) to those employing g-CN prepared with more complex procedures such as
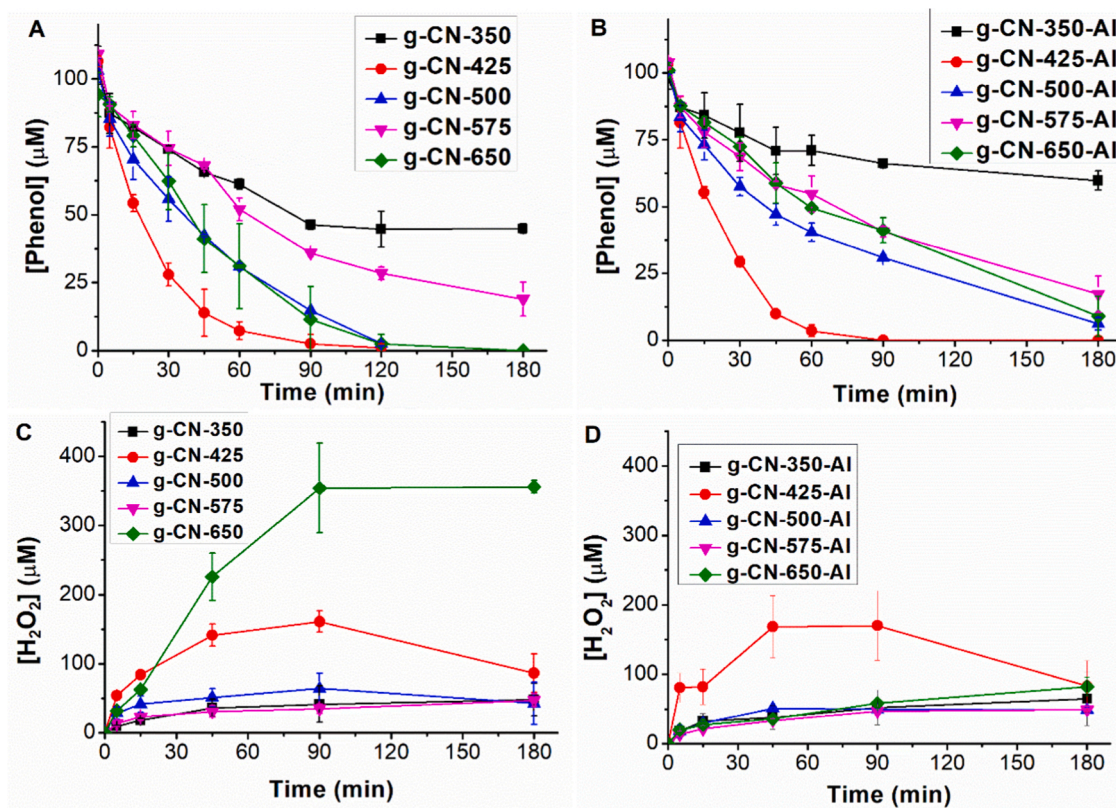
Fig. 6. Phenol 100 μM oxidation results (amount of photocatalyst, 1.65 g L^{-1}, initial pH = 6.0) with UVA irradiation. A) and B) phenol degradation kinetics with g-CN-T and g-CN-T-Al series, respectively; C) and D) H$_2$O$_2$ parallel formation with g-CN-T and g-CN-T-Al series, respectively.

two calcination steps or doping with other elements [58,59]. Furthermore, since HO$_2^\bullet$/O$_2^{\bullet-}$ are reported as main reactive oxygen species responsible of pollutants oxidation with g-CN [14], it is logical to observe faster oxidations with the materials that have the greater photocatalytic activity towards O$_2$ reduction. In this case, although true for g-CN-425, the DoS at potentials for HO$_2^\bullet$ and O$_2^{\bullet-}$ generation with g-CN-425-Al were not in line with the experimental results (Fig. 1E-H).

On the other hand, except for melam oligomers materials (g-CN-350 (-Al)), which led to very slow degradation kinetics ($> 8 \times 10^{-3}$ min^{-1}), the ones prepared from 500 – 650 ºC caused comparable phenol oxidation kinetics, being faster in the cases prepared in open crucibles. Phenol oxidation kinetic rate constants are shown in Table S3.

The H$_2$O$_2$ parallel formation was also measured. Differently than with CH$_3$OH 3 M (Fig. 4), g-CN-650 produced higher H$_2$O$_2$ than g-CN-425, being of 350 and 175 μM in 90 min, respectively (see Fig. 6C). This behaviour can be explained by the fact that the type of hole scavenger can affect the photocatalytic performance of a semiconductor [60,61]. In this case, phenol can interact with g-CN-650 structure more easily than methanol, which does not exhibit the π-π interactions with the photocatalyst. Since hole scavenger is a surface transfer effect, this can also explain the higher production of H$_2$O$_2$ with lower concentration in the case of phenol than in the case of methanol [58,62]. Moreover, since methanol was present in a concentration 3×10^4 times higher than that of phenol, another possibility is that an excess of hole scavenger could have been counterproductive in the photo-production of H$_2$O$_2$ by g-CN-650 due to the plausible oxidation of water: i) with a probe excess, this one consumes most of the photogenerated holes, generating oxidation by-products instead of H$_2$O$_2$, ii) with a probe lack, although H$_2$O$_2$ will be generated from water oxidation, the subsequent H$_2$O$_2$ oxidation will be also higher. In the case of g-CN-425 (more polar and with lower aromaticity), this interaction difference between the photocatalyst surface and the probe should be less important, as well as its ability to oxidise water into H$_2$O$_2$ also lower. These aspects are later discussed in section 3.4.

In agreement with the aforementioned arguments, it can be observed that H$_2$O$_2$ is formed and afterwards consumed (see Fig. 6C and D), differently from the case of methanol 3 M. This effect is in line with phenol kinetics: as soon as the phenol concentration is below 10 μM, the H$_2$O$_2$ is being oxidised, evidencing the lack of hole scavenger. Therefore, it is logical to observe that the H$_2$O$_2$ consumption is mostly evidenced in the cases where phenol oxidation was faster (i.e., g-CN-425(-Al), g-CN-500 and g-CN-650).

3.3.2. Visible light irradiation

When changing from UVA to the visible system, the overall kinetics (phenol oxidation and concomitant H$_2$O$_2$ formation) were evidently slower, as well as the effect of E$_g$ was more obvious, observing good photocatalytic performances only in the cases of the heptazine polymers, g-CN-650 and g-CN-650-Al (results shown in Fig. 7). Phenol photocatalytic oxidation rate constants obtained with visible light are listed in Table S3, fitted as zero order kinetic (therefore, degradation rate is independent of pollutant initial concentration) differently from the pseudo-first order employed with UVA.

Comparing results obtained by g-CN-650 (Fig. 7A and C) vs. g-CN-650-Al (Fig. 7B and D), g-CN-650 achieved, within the same period, almost 6 times more H$_2$O$_2$ production (375 μM in 3 h) and twice faster phenol oxidation kinetics (5.1×10^{-3} M min^{-1}) than its analogous prepared in the covered crucibles (64 μM of H$_2$O$_2$ in 3 h and k$_{obs}$ = 2.8×10^{-3} M min^{-1}). Higher photocatalytic activities were observed for amorphous gCN rather than crystalline one in other works too [47].

Finally, it is also worth mentioning that with the visible/g-CN-650/phenol system there was no H$_2$O$_2$ oxidation compared with UVA/g-CN-650/phenol (compare with Fig. 6C), which is in line with the lower photogenerated holes population in the VB under visible light, leading to phenol higher lifetimes and lower H$_2$O$_2$ oxidations. Furthermore, when comparing probes, once again, the use of methanol 3 M reached to lower
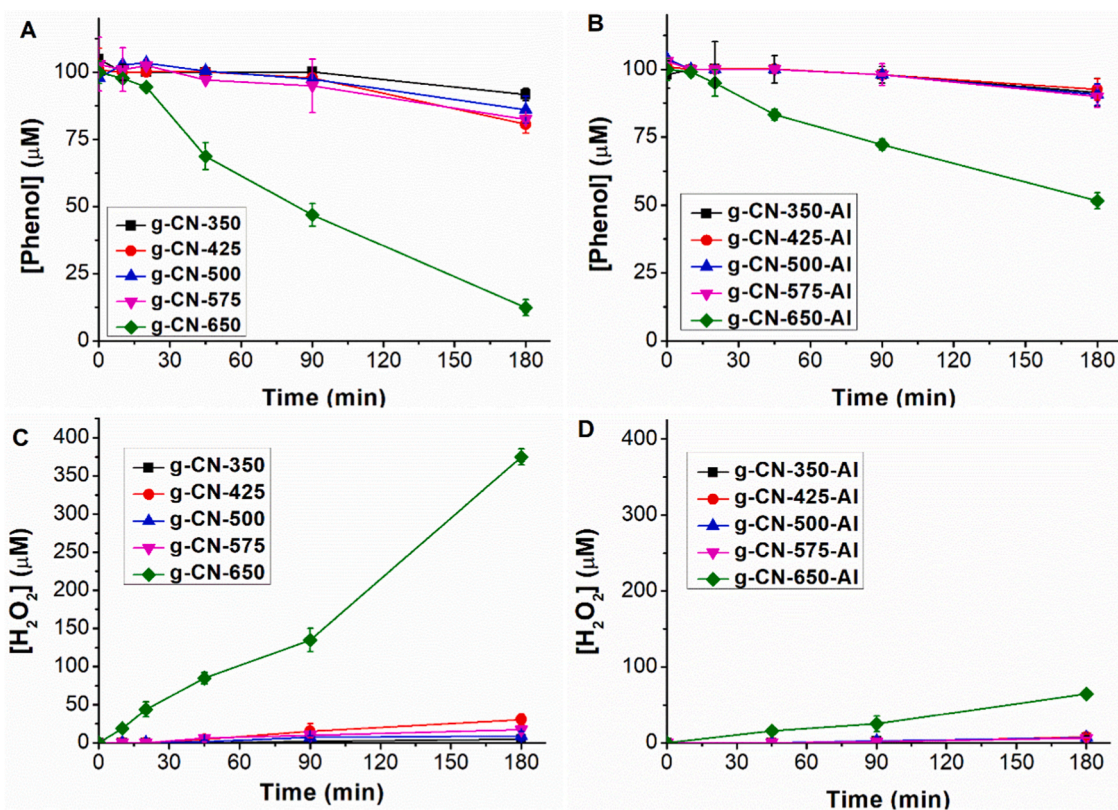
Fig. 7. Phenol 100 μM oxidation results (amount of photocatalyst, 1.65 g L^{-1}, initial pH = 6.0) with visible light irradiation. A) and B) phenol degradation kinetics with g-CN-T and g-CN-T-Al series, respectively; C) and D) H$_2$O$_2$ parallel formation with g-CN-T and g-CN-T-Al series, respectively.

H$_2$O$_2$ production than in the case of phenol 100 μM (Fig. 5 vs. Fig. 7). This suggests that, rather than the nature of the probe as previously hypothesised, an excess of hole scavenger is counterproductive towards H$_2$O$_2$ generation by illuminated g-CN-650, in agreement with the discussion given in section 3.3.1. Therefore, the latter should be able of oxidising water directly into H$_2$O$_2$, being higher in absence of probes (e. g., methanol leading to formaldehyde or formic acid) than water alone (leading to H$_2$O$_2$).

3.4. Water oxidation into H$_2$O$_2$ by g-CN-650

Oxidation of water into H$_2$O$_2$ by g-CN materials has been reported in previous occasions [63,64]. In fact, photo-production of H$_2$O$_2$ obtained in ultra-pure water (in absence of the hole scavengers) under UVA irradiation was <15 μM after 3 h for all the photocatalysts, except for g-CN-650, who reached 35 μM within the same period. A plausible explanation could be that g-CN-650 is more efficient towards oxidising water into H$_2$O$_2$ (its direct oxidation into O$_2$ is less probable as it requires 4 e$^-$) than the others. Noteworthy, these results are opposed to that of DoS, which indicated that g-CN-425 was the one with more oxidative character (Fig. 1G). The hypothesis of water oxidation into H$_2$O$_2$ by g-CN-650 was discussed in section 3.3, where higher H$_2$O$_2$ photoproduction was observed when using phenol 100 μM as hole scavenger than methanol 3 M either with UVA or visible light.

To better understand the behaviour of this photocatalyst, irradiations of g-CN-650 in absence of hole scavengers under aerobic and anaerobic conditions were carried out; visible light was used instead of UVA in order to reduce the oxidation of H$_2$O$_2$ by VB's holes. As shown in Figure S9, the H$_2$O$_2$ photogeneration by visible/g-CN-650 reached the 390 μM at 3 h, slightly higher than in presence of phenol (Fig. 7A), and 50 μM of H$_2$O$_2$ were produced after 3 h of irradiation under anaerobic conditions. Therefore, we propose the following cyclic mechanism for illuminated g-CN-650 under anaerobic conditions: once water is

oxidised into H$_2$O$_2$, the latter acts as source of electrons consumption, being reduced back into H$_2$O. The formed H$_2$O$_2$ should also be oxidised into O$_2$ or HO$_2^\bullet$, these eventually forming again H$_2$O$_2$. H$^+$ might also act as electron scavenger at the beginning of the reaction, but, since H$_2$ formation was not detected and the working pH conditions were ca. 6, this reaction must be of negligible importance.

3.5. Principal Component Analysis: correlations between experimental variables

In order to obtain an overview of the data as a whole, a PCA was carried out. In total, 30 variables were analysed for the series of g-CN-T and g-CN-T-Al (10 materials), all of them listed in Table S3. As shown in Figure S10A-B, six principal components (PC) were enough to explain 95 % of variance, concentrating 40.5 % variance on PC1 and 21.9 % in PC2.

In Fig. 8A, the score plot, it can be stated that PC1 is related with the polymerisation degree and PC2 with the H$_2$O$_2$ photo-production rate, placing g-CN-425-Al as the one with the best performances. Therefore, based on the degree of polymerisation and the photocatalytic performances, the plot can be divided in four regions: region I, oligomeric melam (g-CN-350-Al), with the lowest activity obtained either with UVA or visible light; region II, oligomeric melem (g-CN-350, g-CN-425-Al, g-CN425, g-CN-500-Al), the most photoactive ones, with maximum efficiency if UVA is employed; region III, melon (g-CN-500, g-CN-575, and g-CN-575-Al), with lower photocatalytic activities than those from the former region, but obtaining good H$_2$O$_2$ productions or phenol degradations employing either UVA or visible light; region IV, melon – g-C$_3$N$_4$ (g-CN-650-Al and g-CN-650), explaining results from highly polymerised carbon nitrides, which are useful only if visible light is employed.

Similar results were observed in the score plot of PC1 vs. PC3, the latter seeming to be more related to phenol oxidation rather than H$_2$O$_2$
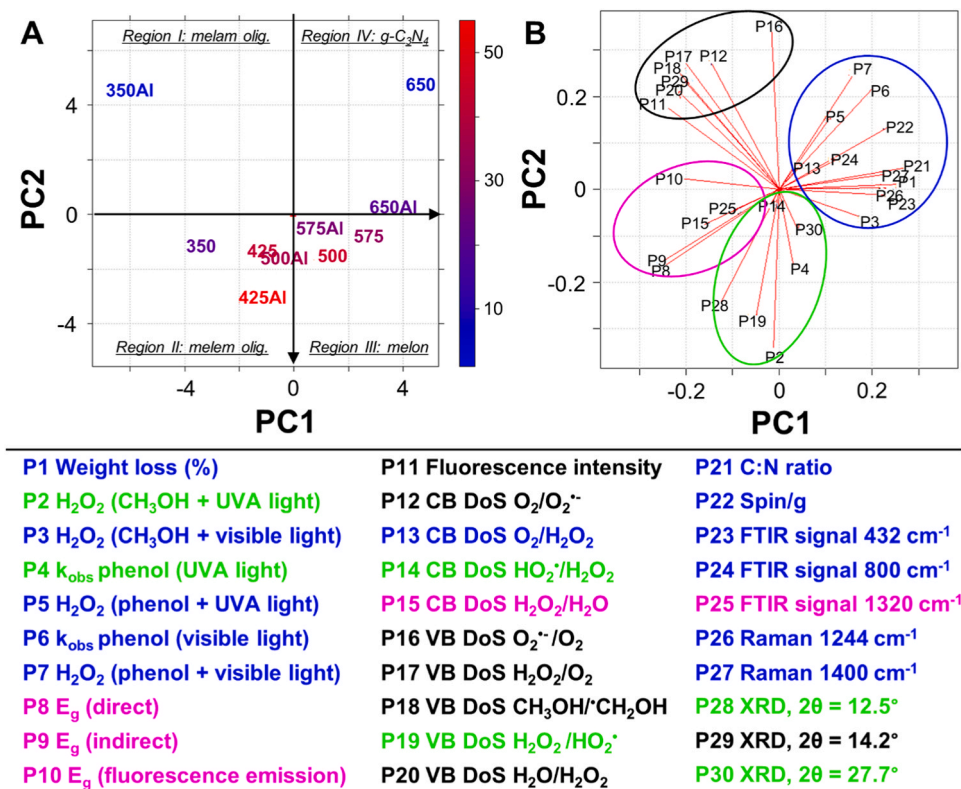
Fig. 8. Principal component analysis results (PC1 vs. PC2) obtained for the different g-CN-T(-Al) materials: A) location of different g-CN-T in the score plot (blue to red scale is based on photogeneration of H_2O_2 under UVA irradiation employing methanol 3 M as hole scavenger); B) loadings plot for the different parameters (P), denoted with an identification number (see inset); parameters clustered together follow a colouring code.

production, since g-CN-425, g-CN-425-Al, g-CN-500 and g-CN-650 were englobed together on the score plot's upper region and the others in the one below (see Figure S10C). Evidently, one should take into account that the explained variance by PC3 is only ≈ 15 %.

Fig. 8B shows the positions of the 30 studied parameters in the PC1 vs. PC2 space. Based on the obtained results, the characterisations correlated (and anti-correlated) with the H_2O_2 photo-generation and phenol oxidation rates under UVA light (variables named as P2 and P4, respectively) were cyclic voltammetry, fluorescence intensity, and XRD (variables englobed within the green and black clusters in the figure). This is in line with the observations made that lower E_g or C:N ratios (i.e. higher polymerisation degrees) were not related with higher photo-catalytic activities. Therefore, by reducing the melam content (charac-teristic diffraction peak at $2\theta = 14.2°$ [53]) while enhancing formation of heptazine units (diffraction peaks at 12.5° and 27.7° [22]), which diminish the fluorescence intensity, will lead to semiconductors with optimal CB and VB towards photo-production of H_2O_2 and pollutants oxidation under UVA light. Furthermore, observing the position along PC2 of the aforementioned variables, P28 (melem diffraction peak at 12.5°) is among the one with the higher weights. This suggests that if the semiconductor is melon enriched (evidenced by observing a decrease in the XRD diffraction at 12.5°, see Fig. 3F), the photocatalytic activity of the resulting material towards the desired reactions will be low under UVA irradiation. P19 (DoS for H_2O_2 oxidation into $HO_2^{\bullet}$) has also a high weight in PC2; however, its location in the diagram was influenced by the outlier of g-CN-350-Al, in line with the opposed position of P16 (oxidation of $O_2^{\bullet-}$ into O_2). As shown in Fig. 1H, g-CN-350-Al exhibited the greatest DoS value for P19 and the lowest for P16, explaining the observed data (g-CN-350-Al was the material with the worst photo-catalytic performances).

Regarding the photocatalytic performance under visible light (P3, P6 and P7), and the H_2O_2 under UVA with phenol 100 μM as hole scavenger (P5), results were aligned with those coming from E_g calculations, C:N

ratio, spin counting, FTIR, and FT-Raman results (i.e., higher synthesis temperature), in concordance with the expectations (see blue and magenta clusters). Noteworthy, if analysing the analogous plot, but against PC3 instead of PC2 (Figure S10D), the oxidation of phenol and H_2O_2 photoproduction under UVA light (P4 and P5, respectively) were correlated with the DoS of O_2 reduction into H_2O_2 (P13) and anti-correlated with melon 27.7° diffraction signal (P30), which is in line with the discussion given above about the higher photocatalytic activity of melem oligomers over melon with UVA light, and also is in line with the higher activity of melon amorphous phase (g-CN-650) than crys-talline one (g-CN-650-Al).

4. Conclusions

Our results highlight significantly better photocatalytic perfor-mances under UVA light (by means of H_2O_2 photo-generation and phenol oxidation rates, respectively) when employing low molecular weight carbon nitrides (oligomeric melem) than with the highly poly-merised ones (melon or g-C_3N_4). Furthermore, the use of crucibles covers (in our case an aluminium foil) greatly enhanced the synthesis yields as well as avoided a higher polymerisation degree at the same applied calcination temperature. For these reasons, g-CN-425-Al seems to be the most convenient photocatalyst to employ in future works.

When changing the light source to visible-LED, the effect of lower E_g was more evident, observing better photocatalytic performances for those prepared at higher temperatures, in line with the extended liter-ature. Consequently, if the prepared photocatalyst has the only aim of being useful with visible light, high synthetic temperature (ca. 650 °C) and plausibly complex synthetic processes will be required. The same line of reasoning applies for developing g-CN materials able of produc-ing H_2O_2 from direct oxidation of water (absence of hole scavengers), in our work only observed for the photocatalyst with the most g-C_3N_4 marked character, the g-CN-650.

Towards a near future of green energy production, the use of UV light should be more convenient from an economic and environmental point of view, allowing to drive photochemical reactions even in regions with few daylight, as well as the costs of LED-UV will decrease due to their increasing global production. Therefore, the preparation of melem-based carbon nitrides will reflect on a considered cost reduction because of their higher photocatalytic activities, the lower energy consumption requested for their preparation, and of the higher synthesis yields. In future works, the here proposed change of focus towards UV/oligomeric melem processes might be analysed from a life cycle assessment perspective to confirm these hypotheses, as well a proper stability study carried out to test if melem is less (or more) stable with respect to melon/graphitic carbon nitride.

Besides the complex synthesis to drive photocatalytic reactions with visible light, another issue related to unnecessary efforts with g-CN works is the use of several characterisation techniques, not always available in all laboratories. The performed PCA (which was detrimental to understand the results obtained in this work) showed that only with a XRD analysis could had been enough to explain, and probably also predict, the H_2O_2 production and/or the phenol degradation rates with UVA light. An analogous argument can be given with visible light performances, as diffuse reflectance or fluorescence spectroscopies could have been sufficient to understand the g-CN that was prepared and explain the obtained photocatalytic performances. Evidently, this mostly applies to well-known carbon nitrides materials as the ones here employed (melam, melem, melon), and not to innovative and complex g-CN-based materials.

CRediT authorship contribution statement

Iván Sciscenko: Writing – review & editing, Writing – original draft, Visualization, Project administration, Methodology, Investigation, Funding acquisition, Formal analysis, Data curation, Conceptualization. **Enrico Salvadori:** Writing – review & editing, Formal analysis, Data curation. **Arianna Actis:** Writing – review & editing, Investigation, Formal analysis, Data curation. **Marco Minella:** Writing – review & editing, Writing – original draft, Visualization, Supervision, Resources, Project administration, Funding acquisition, Formal analysis, Data curation, Conceptualization. **Antonio Arques:** Writing – review & editing, Supervision, Project administration, Funding acquisition. **Fabrizio Sordello:** Writing – review & editing, Formal analysis, Data curation. **Claudio Minero:** Writing – review & editing, Resources, Project administration, Funding acquisition.

Declaration of Competing Interest

The authors declare that they have no known competing financial interests or personal relationships that could have appeared to influence the work reported in this paper.

Data availability

Data will be made available on request.

Acknowledgements

Appendix A. Supporting information

Supplementary data associated with this article can be found in the online version at doi:10.1016/j.jece.2024.114093.

References

[1] F. Sordello, P. Calza, C. Minero, S. Malato, M. Minella, More than one century of history for photocatalysis, from past, present and future perspectives, Catalysts 12 (2022) 1572, https://doi.org/10.3390/catal12121572.

[2] X. Wang, S. Blechert, M. Antonietti, Polymeric graphitic carbon nitride for heterogeneous photocatalysis, ACS Catal. 2 (2012) 1596–1606, https://doi.org/10.1021/cs300240x.

[3] M. Ismael, Y. Wu, A mini-review on the synthesis and structural modification of g-C3N4-based materials, and their applications in solar energy conversion and environmental remediation, Sustain. Energy Fuels. 3 (2019) 2907–2925, https://doi.org/10.1039/c9se00422j.

[4] B. Wang, M. Anpo, X. Wang, Visible Light-Responsive Photocatalysts—From TiO2 to Carbon Nitrides and Boron Carbon Nitride, Elsevier Ltd, 2018, https://doi.org/10.1016/bs.adioch.2018.05.008.

[5] S. Asadzadeh-Khaneghah, A. Habibi-Yangjeh, g-C3N4/carbon dot-based nanocomposites serve as efficacious photocatalysts for environmental purification and energy generation: a review, J. Clean. Prod. 276 (2020) 124319, https://doi.org/10.1016/j.jclepro.2020.124319.

[6] T.S. Miller, A.B. Jorge, T.M. Suter, A. Sella, F. Corà, P.F. McMillan, Carbon nitrides: synthesis and characterization of a new class of functional materials, Phys. Chem. Chem. Phys. 19 (2017) 15613–15638, https://doi.org/10.1039/c7cp02711g.

[7] M. Minella, F. Sordello, C. Minero, Graphitic carbon nitride-based metal-free photocatalyst. in: Mater. Sci. Photocatal., Elsevier, 2021, pp. 449–484, https://doi.org/10.1016/B978-0-12-821859-4.00025-8.

[8] J. Zhu, P. Xiao, H. Li, S.A.C. Carabineiro, Graphitic carbon nitride: synthesis, properties, and applications in catalysis, ACS Appl. Mater. Interfaces 6 (2014) 16449–16465, https://doi.org/10.1021/am502925j.

[9] P. Niu, G. Liu, H.M. Cheng, Nitrogen vacancy-promoted photocatalytic activity of graphitic carbon nitride, J. Phys. Chem. C. 116 (2012) 11013–11018, https://doi.org/10.1021/jp301026y.

[10] C. Huang, Y. Wen, J. Ma, D. Dong, Y. Shen, S. Liu, H. Ma, Y. Zhang, Unraveling fundamental active units in carbon nitride for photocatalytic oxidation reactions, Nat. Commun. 12 (2021) 320, https://doi.org/10.1038/s41467-020-20521-5.

[11] X. Wu, X. Wang, F. Wang, H. Yu, Soluble g-C3N4 nanosheets: facile synthesis and application in photocatalytic hydrogen evolution, Appl. Catal. B Environ. 247 (2019) 70–77, https://doi.org/10.1016/j.apcatb.2019.01.088.

[12] Z. Haider, H. In Cho, G. Hee Moon, H. Il Kim, Minireview: selective production of hydrogen peroxide as a clean oxidant over structurally tailored carbon nitride photocatalysts, Catal. Today 335 (2019) 55–64, https://doi.org/10.1016/j.cattod.2018.11.067.

[13] R.L. Timoner, A. Arques, A.M. Amat, J. Plaza, A. Arencibia, M.J. López-Muñoz, Use of graphitic carbon nitrides as solar-light-driven photocatalysts for the reduction of p-nitrobenzoic acid, Catal. Today 434 (2024) 114674, https://doi.org/10.1016/j.cattod.2024.114674.

[14] I. Velo-Gala, A. Torres-Pinto, C.G. Silva, B. Ohtani, A.M.T. Silva, J.L. Faria, Graphitic carbon nitride photocatalysis: the hydroperoxyl radical role revealed by kinetic modelling, Catal. Sci. Technol. 11 (2021) 7712–7726, https://doi.org/10.1039/d1cy01657a.

[15] A. Torres-Pinto, M.J. Sampaio, C.G. Silva, J.L. Faria, A.M.T. Silva, Recent strategies for hydrogen peroxide production by metal-free carbon nitride photocatalysts, Catalysts 9 (2019), https://doi.org/10.3390/catal9120990.

[16] X. Xu, Y. Sui, W. Chen, W. Huang, X. Li, Y. Li, D. Liu, S. Gao, W. Wu, C. Pan, H. Zhong, H.R. Wen, M. Wen, The photocatalytic H2O2 production by metal-free photocatalysts under visible-light irradiation, Appl. Catal. B Environ. 341 (2024) 123271, https://doi.org/10.1016/j.apcatb.2023.123271.

[17] L. Jiang, X. Yuan, Y. Pan, J. Liang, G. Zeng, Z. Wu, H. Wang, Doping of graphitic carbon nitride for photocatalysis: a reveiw, Appl. Catal. B Environ. 217 (2017) 388–406, https://doi.org/10.1016/j.apcatb.2017.06.003.

[18] L. Li, H. Zhang, F. Ye, Z. Xiao, Z. Zeng, H. Li, M. Ahmad, S. Wang, Q. Zhang, Few-layer meets crystalline structure: collaborative efforts for improving photocatalytic H 2 O 2 generation over carbon nitride, ACS Appl. Mater. Interfaces 16 (2024) 17506–17516, https://doi.org/10.1021/acsami.3c19464.

[19] Y. Shiraishi, Y. Kofuji, H. Sakamoto, S. Tanaka, S. Ichikawa, T. Hirai, Effects of surface defects on photocatalytic H2O2 production by mesoporous graphitic carbon nitride under visible light irradiation, ACS Catal. 5 (2015) 3058–3066, https://doi.org/10.1021/acscatal.5b00408.

[20] H. Liang, H. Wang, A. Wang, R. Cheng, S. Jing, F. Chen, P. Kannan, G. Balkourani, P. Tsiakaras, Efficient photocatalytic hydrogen peroxide production over S-scheme In2S3/molten salt modified C3N5 heterojunction, J. Colloid Interface Sci. 669 (2024) 506–517, https://doi.org/10.1016/j.jcis.2024.04.114.

[21] L. Knapp, E. O'Shaughnessy, J. Heeter, S. Mills, J.M. DeCicco, Will consumers really pay for green electricity? Comparing stated and revealed preferences for residential programs in the United States, Energy Res. Soc. Sci. 65 (2020) 101457, https://doi.org/10.1016/j.erss.2020.101457.

[22] V.W.H. Lau, M.B. Mesch, V. Duppel, V. Blum, J. Senker, B.V. Lotsch, Low-molecular-weight carbon nitrides for solar hydrogen evolution, J. Am. Chem. Soc. 137 (2015) 1064–1072, https://doi.org/10.1021/ja511802c.

[23] T. Dong, G. Dong, K. Han, C. Chen, J. Hu, K. Uvdal, All-organic heterojunctions used for the excellent photocatalytic H2O2 synthesis: the key role of bay-position Cl in PDI, Appl. Catal. B Environ. 354 (2024) 124144, https://doi.org/10.1016/j.apcatb.2024.124144.

[24] S. Goldstein, D. Aschengrau, Y. Diamant, J. Rabani, Photolysis of aqueous H 2 O 2: quantum yield and applications for polychromatic UV actinometry in photoreactors, Environ. Sci. Technol. 41 (2007) 7486–7490, https://doi.org/10.1021/es071379t.

[25] F. Chen, L.-L. Liu, J.-J. Chen, W.-W. Li, Y.-P. Chen, Y.-J. Zhang, J.-H. Wu, S.-C. Mei, Q. Yang, H.-Q. Yu, Efficient decontamination of organic pollutants under high salinity conditions by a nonradical peroxymonosulfate activation system, Water Res 191 (2021) 116799, https://doi.org/10.1016/j.watres.2020.116799.

[26] T. Botari, W.P. Huhn, V.W. Lau, B.V. Lotsch, V. Blum, Thermodynamic equilibria in carbon nitride photocatalyst materials and conditions for the existence of graphitic carbon nitride g-C 3 N 4, Chem. Mater. 29 (2017) 4445–4453, https://doi.org/10.1021/acs.chemmater.7b00965.

[27] F. Saidi, S. Khetari, I.S. Yahia, H.Y. Zahran, T. Hidouri, N. Ameur, The use of principal component analysis (PCA) and partial least square (PLS) for designing new hard inverse perovskites materials, Comput. Condens. Matter 31 (2022) e00667, https://doi.org/10.1016/j.cocom.2022.e00667.

[28] X. Zhang, C. Li, J. Liang, S. Yang, F. Yuan, S. Zheng, J. Yi, Z. Sun, Catalytic membrane with multiscale iron-based catalysts anchored on 2D/2D hybrid g-C3N4/layered clay for pollutant removal, J. Memb. Sci. 685 (2023) 121924, https://doi.org/10.1016/j.memsci.2023.121924.

[29] F. Sordello, I. Berruti, C. Gionco, M.C. Paganini, P. Calza, C. Minero, Photocatalytic performances of rare earth element-doped zinc oxide toward pollutant abatement in water and wastewater, Appl. Catal. B Environ. 245 (2019) 159–166, https://doi.org/10.1016/j.apcatb.2018.12.053.

[30] G. Capilli, M. Costamagna, F. Sordello, C. Minero, Synthesis, characterization and photocatalytic performance of p-type carbon nitride, Appl. Catal. B Environ. 242 (2019) 121–131, https://doi.org/10.1016/j.apcatb.2018.09.057.

[31] A. Actis, P. Fornasiero, M. Chiesa, E. Salvadori, Photo-induced radicals in carbon nitride and their magnetic signature, ChemPhotoChem (2023), https://doi.org/10.1002/cptc.202300203.

[32] H. Zhang, A. Yu, Photophysics and photocatalysis of carbon nitride synthesized at different temperatures, J. Phys. Chem. C. 118 (2014) 11628–11635, https://doi.org/10.1021/jp503477x.

[33] V. Vojinović, A. Azevedo, V.C. Martins, J.M. Cabral, T. Gibson, L. Fonseca, Assay of H2O2 by HRP catalysed co-oxidation of phenol-4-sulphonic acid and 4-aminoantipyrine: characterisation and optimisation, J. Mol. Catal. B Enzym. 28 (2004) 129–135, https://doi.org/10.1016/j.molcatb.2004.02.003.

[34] V. Maurino, M. Minella, F. Sordello, C. Minero, A proof of the direct hole transfer in photocatalysis: the case of melamine, Appl. Catal. A Gen. 521 (2016) 57–67, https://doi.org/10.1016/j.apcata.2015.11.012.

[35] F. Sordello, F. Pellegrino, M. Prozzi, C. Minero, V. Maurino, Controlled periodic illumination enhances hydrogen production by over 50% on Pt/TiO2, ACS Catal. 11 (2021) 6484–6488, https://doi.org/10.1021/acscatal.1c01734.

[36] R. Leardi, C. Melzi, G. Polotti, CAT (Chemometric Agile Tool), freely downloadable, (n.d.). ⟨http://gruppochemiometria.it/index.php/software⟩ (accessed July 4, 2023).

[37] H. Yan, Y. Chen, S. Xu, Synthesis of graphitic carbon nitride by directly heating sulfuric acid treated melamine for enhanced photocatalytic H 2 production from water under visible light, Int. J. Hydrog. Energy 37 (2012) 125–133, https://doi.org/10.1016/j.ijhydene.2011.09.072.

[38] P. Makuła, M. Pacia, W. Macyk, How to correctly determine the band gap energy of modified semiconductor photocatalysts based on UV-vis spectra, J. Phys. Chem. Lett. 9 (2018) 6814–6817, https://doi.org/10.1021/acs.jpclett.8b02892.

[39] M.C. Barreto, R.G. Braga, S.G. Lemos, W.D. Fragoso, Determination of melamine in milk by fluorescence spectroscopy and second-order calibration, Food Chem. 364 (2021) 130407, https://doi.org/10.1016/j.foodchem.2021.130407.

[40] F. Sordello, C. Minero, G. Viscardi, P. Quagliotto, Highly photoactive polythiophenes obtained by electrochemical synthesis from bipyridine-containing terthiophenes, Energies 12 (2019), https://doi.org/10.3390/en12030341.

[41] S.A. Shevlin, Z.X. Guo, Anionic dopants for improved optical absorption and enhanced photocatalytic hydrogen production in graphitic carbon nitride, Chem. Mater. 28 (2016) 7250–7256, https://doi.org/10.1021/acs.chemmater.6b02002.

[42] H.R.S. Abdellatif, G. Zhang, X. Wang, D. Xie, J.T.S. Irvine, J. Ni, C. Ni, Boosting photocatalytic oxidation on graphitic carbon nitride for efficient photocatalysis by heterojunction with graphitic carbon units, Chem. Eng. J. 370 (2019) 875–884, https://doi.org/10.1016/j.cej.2019.03.266.

[43] J.J. Pignatello, E. Oliveros, A. MacKay, Advanced oxidation processes for organic contaminant destruction based on the Fenton reaction and related chemistry, Crit. Rev. Environ. Sci. Technol. 36 (2006) 1–84, https://doi.org/10.1080/10643380500326564.

[44] M. Marchi, E. Raciti, S.M. Gali, F. Piccirilli, H. Vondracek, A. Actis, E. Salvadori, C. Rosso, A. Criado, C. D'Agostino, L. Forster, D. Lee, A.C. Foucher, R.K. Rai, D. Beljonne, E.A. Stach, M. Chiesa, R. Lazzaroni, G. Filippini, M. Prato, M. Melchionna, P. Fornasiero, Carbon vacancies steer the activity in dual Ni carbon nitride photocatalysis, Adv. Sci. 2303781 (2023) 1–12, https://doi.org/10.1002/advs.202303781.

[45] M.M. Roessler, E. Salvadori, Principles and applications of EPR spectroscopy in the chemical sciences, Chem. Soc. Rev. 47 (2018) 2534–2553, https://doi.org/10.1039/c6cs00565a.

[46] Q. Gu, Z. Gao, H. Zhao, Z. Lou, Y. Liao, C. Xue, Temperature-controlled morphology evolution of graphitic carbon nitride nanostructures and their photocatalytic activities under visible light, RSC Adv. 5 (2015) 49317–49325, https://doi.org/10.1039/C5RA07284K.

[47] F. Longobardo, G. Gentile, A. Criado, A. Actis, S. Colussi, V. Dal Santo, M. Chiesa, G. Filippini, P. Fornasiero, M. Prato, M. Melchionna, Tailored amorphization of graphitic carbon nitride triggers superior photocatalytic C–C coupling towards the synthesis of perfluoroalkyl derivatives, Mater. Chem. Front. 5 (2021) 7267–7275, https://doi.org/10.1039/D1QM01077H.

[48] A. Actis, M. Melchionna, G. Filippini, P. Fornasiero, M. Prato, E. Salvadori, M. Chiesa, Morphology and light-dependent spatial distribution of spin defects in carbon nitride, Angew. Chem. 134 (2022), https://doi.org/10.1002/ange.202210640.

[49] X. Li, J. Zhang, L. Shen, Y. Ma, W. Lei, Q. Cui, G. Zou, Preparation and characterization of graphitic carbon nitride through pyrolysis of melamine, Appl. Phys. A Mater. Sci. Process. 94 (2009) 387–392, https://doi.org/10.1007/s00339-008-4816-4.

[50] B.V. Lotsch, W. Schnick, From triazines to heptazines: novel nonmetal tricyanomelaminates as precursors for graphitic carbon nitride materials, Chem. Mater. 18 (2006) 1891–1900, https://doi.org/10.1021/cm052342f.

[51] S.C. Yan, Z.S. Li, Z.G. Zou, Photodegradation performance of g-C3N4 fabricated by directly heating melamine, Langmuir 25 (2009) 10397–10401, https://doi.org/10.1021/la900923z.

[52] E. Wirnhier, M.B. Mesch, J. Senker, W. Schnick, Formation and characterization of melam, melam hydrate, and a melam–melem adduct, Chem. Eur. J. 19 (2013) 2041–2049, https://doi.org/10.1002/chem.201203340.

[53] B.V. Lotsch, W. Schnick, New light on an old story: formation of melam during thermal condensation of melamine, Chem. – A Eur. J. 13 (2007) 4956–4968, https://doi.org/10.1002/chem.200601291.

[54] H. Zhao, Q. Jin, M.A. Khan, S. Larter, S. Siahrostami, M.G. Kibria, J. Hu, Rational design of carbon nitride for remarkable photocatalytic H2O2 production, Chem. Catal. 2 (2022) 1720–1733, https://doi.org/10.1016/j.checat.2022.04.015.

[55] P. Zhang, Y. Tong, Y. Liu, J.J.M. Vequizo, H. Sun, C. Yang, A. Yamakata, F. Fan, W. Lin, X. Wang, W. Choi, Heteroatom dopants promote two-electron O 2 reduction for photocatalytic production of H 2 O 2 on polymeric carbon nitride, Angew. Chem. 132 (2020) 16343–16351, https://doi.org/10.1002/ange.202006747.

[56] Z. Wei, M. Liu, Z. Zhang, W. Yao, H. Tan, Y. Zhu, Efficient visible-light-driven selective oxygen reduction to hydrogen peroxide by oxygen-enriched graphitic carbon nitride polymers, Energy Environ. Sci. 11 (2018) 2581–2589, https://doi.org/10.1039/c8ee01316k.

[57] J. Xiao, Q. Han, Y. Xie, J. Yang, Q. Su, Y. Chen, H. Cao, Is C3N4 chemically stable toward reactive oxygen species in sunlight-driven water treatment, Environ. Sci. Technol. 51 (2017) 13380–13387, https://doi.org/10.1021/acs.est.7b04215.

[58] A. Torres-Pinto, M.J. Sampaio, C.G. Silva, J.L. Faria, A.M.T. Silva, Metal-free carbon nitride photocatalysis with in situ hydrogen peroxide generation for the degradation of aromatic compounds, Appl. Catal. B Environ. 252 (2019) 128–137, https://doi.org/10.1016/j.apcatb.2019.03.040.

[59] J. Lin, W. Tian, Z. Guan, H. Zhang, X. Duan, H. Wang, H. Sun, Y. Fang, Y. Huang, S. Wang, Functional carbon nitride materials in photo-fenton-like catalysis for environmental remediation, Adv. Funct. Mater. 32 (2022), https://doi.org/10.1002/adfm.202201743.

[60] R. Djellabi, M.F. Ghorab, Photoreduction of toxic chromium using TiO2-immobilized under natural sunlight: effects of some hole scavengers and process parameters, Desalin. Water Treat. 55 (2015) 1900–1907, https://doi.org/10.1080/19443994.2014.927335.

[61] Y. Chu, X. Zheng, J. Fan, Preparation of sodium and boron co-doped graphitic carbon nitride for the enhanced production of H2O2 via two-electron oxygen reduction and the degradation of 2,4-DCP via photocatalytic oxidation coupled with Fenton oxidation, Chem. Eng. J. 431 (2022) 134020, https://doi.org/10.1016/j.cej.2021.134020.

[62] A. Ben-Refael, I. Benisti, Y. Paz, Transient photoinduced phenomena in graphitic carbon nitride as measured at nanoseconds resolution by step-scan FTIR, Catal. Today 340 (2020) 97–105, https://doi.org/10.1016/j.cattod.2018.11.010.

[63] Z. Zhu, H. Pan, M. Murugananthan, J. Gong, Y. Zhang, Visible light-driven photocatalytically active g-C3N4 material for enhanced generation of H2O2, Appl. Catal. B Environ. 232 (2018) 19–25, https://doi.org/10.1016/j.apcatb.2018.03.035.

[64] Y. Shiraishi, S. Kanazawa, Y. Kofuji, H. Sakamoto, S. Ichikawa, S. Tanaka, T. Hirai, Sunlight-driven hydrogen peroxide production from water and molecular oxygen by metal-free photocatalysts, Angew. Chem. Int. Ed. 53 (2014) 13454–13459, https://doi.org/10.1002/anie.201407938.